



pubs.acs.org/Biomac Article

# Environmentally Benign Nanoantibiotics with a Built-in Deactivation Switch Responsive to Natural Habitats

Wan Zheng, Miguel Anzaldua, Ankita Arora, Yunjiang Jiang, Kelly McIntyre, Michael Doerfert, Theodora Winter, Abhijit Mishra, Hairong Ma, and Hongjun Liang\*



Cite This: Biomacromolecules 2020, 21, 2187-2198



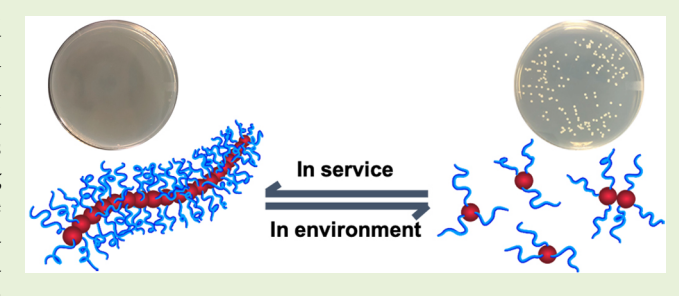
**ACCESS** I

III Metrics & More

Article Recommendations

si Supporting Information

ABSTRACT: The massive use of antibiotics in healthcare and agriculture has led to their artificial accumulation in natural habitats, which risks the structure and function of the microbial communities in ecosystems, threatens food and water security, and accelerates the development of resistome. Ideally, antibiotics should remain fully active in clinical services while becoming deactivated rapidly once released into the environment, but none of the current antibiotics meet this criterion. Here, we show a nanoantibiotic design that epitomizes the concept of carrying a built-in "OFF" switch responsive to natural stimuli. The environ-



mentally benign nanoantibiotics consist of cellulose backbones covalently grafted with hydrophilic polymer brushes that by themselves are antimicrobially inactive. In their nanostructured forms in services, these cellulose-based polymer molecular brushes are potent killers for both Gram-positive and Gram-negative bacteria, including clinical multidrug-resistant strains; after services and being discharged into the environment, they are shredded into antimicrobially inactive pieces by cellulases that do not exist in the human body but are abundant in natural habitats. This study illuminates a new concept of mitigating the environmental footprints of antibiotics with rationally designed nanoantibiotics that can be dismantled and disabled by bioorthogonal chemistry occurring exclusively in natural habitats.

## **■** INTRODUCTION

In the battles against bacterial infections in healthcare and agriculture, antibiotics have been used at a massive scale for many decades. It was estimated that the annual antibiotics consumption reached 100 000-200 000 tons in 2010 worldwide, and up to 90% of the administered antibiotics were discharged directly into the environment in various active forms. 1,2 Since the natural degradation of most antibiotics is an extremely slow process, 1-5 unusually high concentrations of artificial antibiotics were detected in soils and waterways in many parts of the world. 1,2,6-10 Emerging evidence has suggested the dire consequences caused by the increasing accumulation of antibiotic wastes in ecosystems, including short- and long-term adverse effects on the structure and function of microbial communities involved in biogeochemical cycling and organic matter degradation, contamination of water, plants, stockbreeding, and aquaculture products in the food chains, and promoting the development of resistome, i.e., the environmental reservoir of resistance genes shared among pathogenic and nonpathogenic bacteria. 1,2,10-21 Although the concept of biodegradable antibiotics that can break down in vivo has been reported, <sup>22–25</sup> caution should be taken on the potential risks of in vivo degradation, as it may encourage the development of bacterial resistance due to the continuous loss of antimicrobial activity while in use. Other options to mitigate

the antibiotic wastes include innovative sewage management aimed to reduce, capture, or degrade the released antibiotic residues, <sup>26–29</sup> but it is practically challenging to cover the diverse release pathways and match the massive scale of discharged antibiotics. Ideally, antibiotics should remain fully active in clinical services while becoming deactivated rapidly once released into the environment, but none of the current antibiotics possess this desirable feature.

Our recent discovery of phage-mimicking antibiotics revealed an interesting role of nanostructures on defining the antimicrobial activity and selectivity. On one hand, hydrophilic molecules that by themselves are nontoxic but antimicrobially inactive can be transformed into efficacious antibiotics once assembled into distinct nanostructures, because nanostructures give rise to multivalent interactions that induce pore formation exclusively on microbial membranes; on the other hand, nanostructures with well-defined sizes and shapes can recognize the nanoporous cell wall

Received: February 3, 2020 Revised: March 20, 2020 Published: March 23, 2020





difference of bacteria to act with different selectivity. This discovery suggests that nanostructured antibiotics, i.e., nanoantibiotics, have the potential to serve as a generic platform for the design of "smart" antibiotics with in-demand activity and selectivity in response to external stimuli by assembly or disassembly of their nanostructures. Here, we exploit this "plug-to-activate" and "unplug-to-deactivate" concept toward mitigating the environmental footprints of antibiotics with a prototypical design of nanoantibiotics that can be dismantled and disabled by bioorthogonal chemistry occurring exclusively in natural habitats.

### MATERIALS AND METHODS

**Materials.** Cellulose ( $\overline{M}_n \approx 40 \text{ kDa}$ ), N-phenyl-1-naphthylamine (NPN), and N,N-dimethylamino-2-ethyl methacrylate (DMAEMA; 98%) were purchased from Acros Organics (Thermo Fisher Scientific, NJ). Thiazolyl Blue Tetrazolium Bromide (MTT) was purchased from Sigma-Aldrich (St. Louis, MO) and used as received. All other chemicals, unless otherwise specified, were also purchased from Sigma-Aldrich and used as received. DMAEMA was purified by passing through a column packed with base aluminum oxide before use. Coper(I) bromide (CuBr, 99%) was purified by stirring in acetic acid at room temperature overnight and washed with ethanol to a neutral pH. Ionic liquid 1-allyl-3-methylimidazolium chloride (AMIMCl) was synthesized as reported. S1,32

Cellulase from Trichoderma reesei (ATCC26921) (5 units/mg) was purchased from Sigma-Aldrich. 1,2-Dioleoyl-sn-glycero-3-phospho-(1'-rac-glycerol) (sodium salt) (DOPG), 1,2-dioleoyl-sn-glycero-3phosphocholine (DOPC), 1,2-dioleoyl-sn-glycero-3-phosphoethanolamine (DOPE), and 1,2-dioleoyl-sn-glycero-3-phosphoethanolamine-N-(lissamine rhodamine B sulfonyl) (ammonium salt) (18:1 Liss Rhod PE) were purchased from Avanti Lipid (Alabaster, AL) and used as received. E. coli (ATCC 25922) and S. aureus (ATCC 25923) were purchased from American Type Culture Collection (ATCC) (Manassas, VA) and reactivated according to the instructions. Mueller Hinton (MH) broth was purchased from Becton, Dickinson, and Co. (BD) (Franklin Lakes, NJ) and used as received. The clinical multidrug-resistant bacteria strains PA14 and MU50 were kindly provided by Professor Kendra Rumbaugh at TTUHSC. Fresh human red blood cells (HRBCs) were purchased from Innovative Research Inc. (Novi, MI), stored at 4 °C, and used within 2 weeks. The HEK-293 (human embryonic kidney) cells were kindly provided by Professor Min Kang at TTUHSC. Dulbecco's modified Eagle's medium (DMEM, containing 4.5 g/L glucose, L-glutamine, and sodium pyruvate) was purchased from Mediatech, Inc. (Manassas, VA). Trypsin-EDTA (0.25%, phenol red) solution was purchased from Thermo Fisher Scientific (Grand Island, NY)

Enzymatic Degradation of Polymer Molecular Brushes (PMBs). The degradation of cellulose-based PMBs was conducted following a previously reported protocol.<sup>33</sup> As an example, PMBs (50 mg) and cellulase (20 mg) were dissolved in 5 mL of 0.05 M citrate buffer (pH 4.8). The mixture was incubated in an orbital shaker (250 rpm) at 30 °C. After different incubation times, 1.0 mL of sample was taken from the mixture and heated at 100 °C for 15 min to deactivate the enzymes. After cooling down to room temperature, the solution was centrifuged at 10 000 rpm for 5 min using an Eppendorf microcentrifuge to remove the precipitated enzyme. The supernatant was dialyzed against Millipore water to remove residual buffer salt using a dialysis tube (MWCO 500-1000 Da) from Spectrum (Gardena, CA). The resulting solution was lyophilized to obtain the degradation products. We used gel permeation chromatography (GPC) to track the enzymatic degradation at different times and found no difference after 3 h of cellulolysis.

**Intrinsic Viscosity.** The intrinsic viscosity of the linear-chain brush polymer control, PMBs, and degraded PMBs in water at 25 °C was measured using a Cannon–Fenske routine viscometer (Cannon Instrument Co., PA). For each polymer, five solutions in filtered Millipore water with concentrations (c) ranging from 0.2 to 1.0 mg/

mL were prepared. The average flow time for filtered Millipore water was measured in triplicate and used as the reference  $(t_{\rm o})$ . The average flow times of each polymer solution at different concentrations were also measured in triplicate  $(t_{\rm s})$ . The reduced  $(\eta_{\rm red})$  and inherent  $(\eta_{\rm inh})$  viscosity of the polymer solutions were calculated as eqs 1 and 2, respectively.

$$\eta_{\rm red} = \frac{\frac{t_{\rm s}}{t_{\rm o}} - 1}{c} \tag{1}$$

$$\eta_{\rm inh} = \frac{\ln\left(\frac{t_{\rm s}}{t_{\rm o}}\right)}{c} \tag{2}$$

The intrinsic viscosity of each polymer was determined by extrapolating the linear regressions of its reduced and inherent viscosity plotted against its concentrations (i.e., x axis). The intersections on the viscosity axis (i.e., y axis) of both linear regressions are very close to each other, and the intrinsic viscosity was taken as the average of the two.

Bacterial Membrane Permeabilization and Cytoplasmic Release Assays. The bacteria were incubated overnight at 37 °C and diluted into fresh MH broth (100×) to regrow. Bacterial growth was monitored by optical density at  $\lambda = 600$  nm (OD<sub>600</sub>) using a UV-vis spectrometer (IMPLEN OD600, Munich, Germany). After the mid log phase  $(OD_{600} = 0.5-0.6)$  was reached, the bacteria were washed twice with sterile PBS buffer and harvested by centrifugation at 10 000 rpm for 5 min using an Eppendorf microcentrifuge. Finally, the bacterial cells were resuspended in PBS buffer and adjusted to obtain an  $OD_{600}$  of 1.0. The bacterial suspension (400  $\mu$ L) was pipetted into the 1.5 mL Eppendorf tube, and 200  $\mu$ L of either PMBs, degraded PMBs, linear-chain brush polymer control PTMAEMA<sub>32</sub> (10 mg/mL) was added to each tube. Bacterial suspension mixed with PBS buffer without any polymers was used as a negative control, while bacterial suspension mixed with Triton (1.0%) solution was used as a positive control. For the membrane permeabilization assay, NPN (10 μM final concentration) was added into bacterial suspensions kept in the dark prior to adding each polymer (or mixed with the Triton solution in the positive control). The NPN fluorescence change (Ex/ Em = 350/420 nm) was recorded continuously using a F-7000 FL Spectrophotometer (Hitachi, Tokyo, Japan), and time zero was set at the time when individual polymer (or Triton) solution was added into the bacterial suspension.

For the cytoplasmic release assay, all of the bacterial suspensions mixed with individual polymer (or control) solutions were incubated in an orbital shaker at 37 °C for 3 h first, followed by centrifugation at 10 000 rpm for 5 min to remove bacterial cells and/or cell debris. The supernatant was collected for UV—vis measurement, and the final UV—vis spectrum of each sample was obtained by subtracting its blank control. In order to generate the blank control for each sample, its negative control was centrifuged at 10 000 rpm for 5 min to remove the bacterial cells, and the supernatant (400  $\mu \rm L)$  was added with 200  $\mu \rm L$  of the respective polymer (10 mg/mL) solution for that sample.

Cytotoxicity Assays against Mammalian Cells. Besides hemolysis and hemagglutination assays against HRBCs, we also performed both MTT and live/dead cell staining assays against HEK-293 cells by treating the model mammalian cell with PMBs, degraded PMBs, and linear-chain brush polymer control, respectively. For the MTT assay, the HEK-293 cells were grown to ~70% confluence at 37 °C in a 5% CO<sub>2</sub> incubator using a tissue culture dish and DMEM supplemented with 5% fetal calf serum and 0.5% Pen/Strep. After being detached by Trypsin and splitting, the HEK-293 cells were seeded into a 96-well plate at a concentration of  $\sim 5 \times 10^3$  cells/well in fresh DMEM (100  $\mu$ L/well). Seeded cells were incubated at 37 °C in a 5% CO<sub>2</sub> incubator for about 2-3 days until the confluence reach ~70%. A graded concentration series of polymer solutions in PBS buffer (10 mM, pH = 7.4) was prepared and added to appropriate wells in quadruplicate (10  $\mu$ L/well). PBS buffer and 3% Triton (10  $\mu$ L/well) were added as negative and positive controls, respectively.

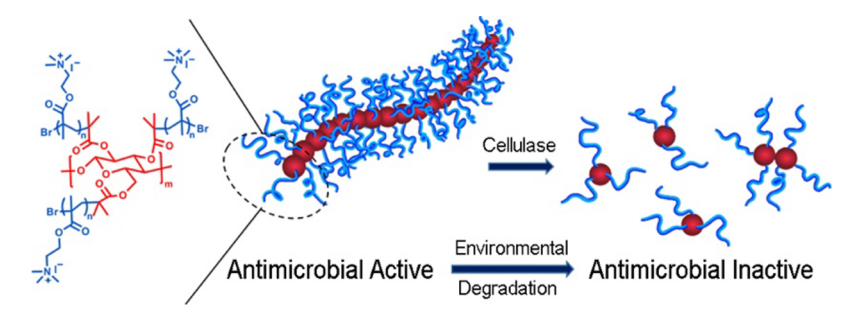


**Figure 1.** Nanoantibiotics with a built-in "OFF" switch responsive to natural stimuli. In service in their nanostructured forms, those cellulose-based PMBs kill both Gram-positive and Gram-negative bacteria including the multidrug-resistant strains with a high potency. After service and being discharged into the environment, they are quickly deactivated by shredding into antimicrobially inactive pieces in the presence of cellulases that do not exist in the human body but are abundant in natural habitats.

After the cells were incubated at 37 °C overnight, the old media with added polymers were replaced by fresh DMEM (100  $\mu$ L/well). MTT in PBS buffer (5 mg/mL, 10  $\mu$ L/well) was added in each well and incubated for another 4 h. After the old medium was removed, 100  $\mu$ L of sterile DMSO was added to dissolve formazan crystals produced by living cells. The optical density was detected at 570 nm using a BioTek Synergy 4 microplate reader (Winooski, VT, USA). Cell viability was determined by normalizing the measured absorbance in polymer-containing wells with the positive and negative controls.

For the live/dead cell staining assay, the HEK-293 cells were seeded into a 24-well plate at a concentration of  $\sim 5 \times 10^3$  cells/well in 100 µL of DMEM. The cells were incubated at 37 °C in a 5% CO<sub>2</sub> incubator for about 2 days until the confluence reached 70%. A graded concentration series of polymer solutions in culture medium was prepared and added to the wells in duplicate (10  $\mu$ L/well). PBS buffer (pH = 7.4) and 3% Triton (10  $\mu$ L/well) were added as negative and positive controls, respectively. After 24 h of incubation, the cell viability was assessed using the Live/Dead Cell Staining Kit (PromoKine PK-CA707-30002) according to the manufacturer's instruction. In brief, adherent cells were rinsed twice with PBS buffer (pH = 7.4), and a sufficient volume (200 uL) of calcein-AM (2  $\mu$ M)/ EthD-III (4  $\mu$ M) staining solution was added to cover the cell monolayer. The cells were stained for 45 min at room temperature, rinsed with PBS buffer twice, and observed under a fluorescence microscope (Zeiss Axiovert 200 M Microscope). While the cellpermeant, nonfluorescent calcein-AM is well retained within live cells and converted to calcein by intracellular esterase to produce an intense uniform green fluorescence (Ex/Em ≈ 495/515 nm), EthD-III enters dead cells with damaged plasma membranes to produce a bright red fluorescence (Ex/Em  $\approx 520/635$  nm) upon binding to nucleic acids.

Other Characterization Methods. The bacterial killing and inhibitory assays, hemolysis and hemagglutination assays, fluorescent dye leakage assay, nuclear magnetic resonance (NMR) and Fourier transform infrared (FTIR) spectroscopy, GPC, scanning electron microscopy (SEM), transmission electron microscopy (TEM), and synchrotron small-angle X-ray scattering (SAXS) studies are as described previously. We also performed SAXS using a custom-designed in-house setup built by Xenocs (Amherst, MA). The inhouse setup is an integrated Xeuss/BioXolver system that consists of an Eiger R 1M hybrid photon-counting detector from Dectris (Baden, Switzerland), a Xenocs GeniX 3D Cu ultralow divergence X-ray source (30 W/40  $\mu$ m) coupled with the FOX3D single-reflection collimating optics, scatterless slits, BioCube, BioXolver, capillary flow cell, and other accessories to operate at (GI)SAXS/USAXS/WAXS modes for both materials science and protein samples.

## ■ RESULTS AND DISCUSSION

Synthesis and Characterization of Environmentally Degradable Nanoantibiotics. Our prototypical nanoantibiotic design is represented by PMBs consisting of cellulose backbones covalently grafted with hydrophilic and antimicro-

bially inactive linear-chain polymer brushes (Figure 1). Cellulose is the most abundant biopolymer in nature. Although cellulases, the enzymes that break down cellulose, do not exist in the human body, they are produced in large quantities in natural habitats by various fungi, bacteria, and protozoans that are nonpathological to humans. In fact, cellulolysis is one of the most executed bioorthogonal chemistry in nature and plays a critical role for the carbon cycle in the biosphere.<sup>34–36</sup>

To prepare the PMBs, we first converted cellulose fibers into macroinitiators for atom transfer radical polymerization (ATRP) of polymer brushes. Due to the extensive H-bonding network among the glucose repeating units joined sequentially via the  $1,4-\beta$ -glycosidic linkages along its chains, cellulose is insoluble in nearly all solvents except for ionic liquids, such as AMIMCl. 37,38 We synthesized the macroinitiator (i.e., cellulose-Br) by reacting cellulose dissolved in AMIMCl with  $\alpha$ -bromoisobutyryl bromide. The resultant cellulose-Br was easily soluble in many polar solvents and was used as a macroinitiator to graft well-defined poly(N,N-dimethylamino-2-ethyl methacrylate) (PDMAEMA) brushes via ATRP. The PDMAEMA brushes were subsequently converted to hydrophilic and cationic poly(N,N,N-trimethylamino-2-ethyl methacrylate) (PTMAEMA) via quaternization.<sup>39</sup> We chose PDMAEMA as a model brush because it is widely used in drug and gene delivery. 40-42 Although PDMAEMA itself showed antimicrobial and hemolytic activities, 43,44 probably due to its amphiphilic and cationic properties reminiscent of the well-recognized antibiotic traits of antimicrobial peptides, 45-47 these activities diminished at increasing degree of quaternization when PDMAEMA was converted to hydrophilic PTMAEMA. 43,48,49 Details of our synthesis and characterization are discussed in the Supporting Information (SI). We used NMR and FTIR spectroscopy, GPC, together with brush cleavage experiments to determine the brush size, graft density, and degree of quaternization and confirmed the successful synthesis of cellulose-g-PTAMEMA<sub>31</sub>, where 31 represents the average degree of polymerization (DP) of the PTMAEMA brushes (Figures S1-S3, Supporting Information). We also synthesized a linear-chain PTMAEMA<sub>32</sub> that has a similar size as the PTMAEMA brushes on the PMBs as a control (Figures S4 and S5, Supporting Information).

The GPC studies of cellulose-Br showed that the commercially available cellulose has a broad range of molecular weight distribution, and this broad size distribution profile carries on after grafting with PDMAEMA brushes (Figure 2a). In contrast to the polydisperse cellulose backbones of PMBs, well-defined PDMAEMA brushes (i.e.,  $DP \approx 31$ ) were

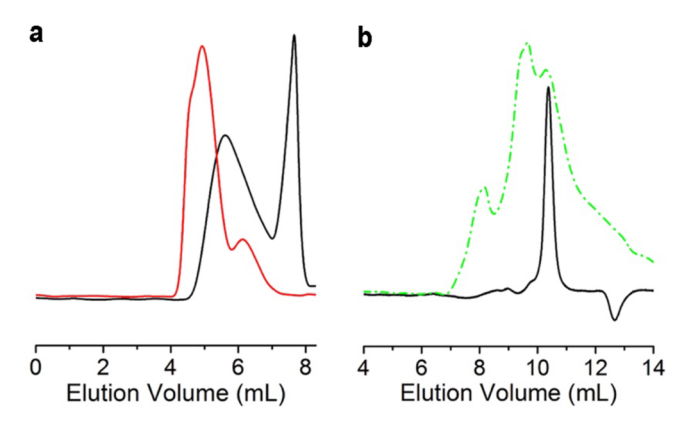


**Figure 2.** Structural evolution of model PMBs from synthesis to degradation as monitored by GPC. (a) Both cellulose-Br (black) and cellulose-g-PDMAEMA $_{31}$  (red) are characterized by similarly profiled broad-size distributions indicative of the polydisperse nature of cellulose (column, Agilent PLgel 5  $\mu$ m MIXED-D; eluent, DMF with 0.02 M ammonium acetate). (b) After cellulase degradation for 3 h, the hydrophilic PMBs are broken into small pieces (dashed green trace), one of which has an elution volume similar to that of the PTMAEMA $_{32}$  control (black trace) (column, Agilent PL aquagel-OH 50; eluent, pH 7.0 buffer with 0.01 M NaH $_2$ PO $_4$  and 0.1 M NaN $_3$ ).

obtained on individual PMBs via ATRP (Figures S1–S3, Supporting Information). After quaternization, the hydrophilic PMBs remained stable by themselves but were quickly degraded (i.e., in 3 h) into small pieces in the presence of cellulase, as shown by the GPC of the degraded products in comparison to that of the PTMAEMA<sub>32</sub> control (Figure 2b). This rapid degradation was further confirmed by viscosity measurements. The intrinsic viscosity of PMBs was measured

as 68.6 mL/g. It dropped to 45.2 mL/g after cellulase degradation for 3 h, approaching that of the PTMAEMA<sub>32</sub> control (i.e., 43.0 mL/g). It should be noted that the cellulolysis assay in the lab mimics the cellulolysis process in nature but differs in both the enzyme and the substrate concentrations. The cellulase concentrations in natural habitats change greatly depending on the types of cellulase-producing microorganisms in a local ecosystem, their number densities and growth cycles, seasonal shifts, and other environmental variables. Although quantitative measurements are difficult, previous studies have indicated that cellulase represents ~20% of the cell mass in some of the cellulase-producing microorganisms such as Clostridium thermocellum, 50 and cellulase activity in soil samples collected during different seasons in the Negev Desert fluctuated between 0 and 16  $\mu$ g of cellulase per gram of soil per hour.<sup>51</sup> The cellulase concentration in rich soils populated with cellulase-producing microorganisms is expected to be higher but likely still ~100× lower than the 4 mg/g concentration used in the lab assay. However, the expected concentrations of antibiotic wastes in the environment would also be hundreds of times lower than that tested in the lab assay (i.e., 10 mg/g of the PMBs). As such, the cellulolysis assay in the lab is still relevant and suggests that the PMBs, if used as antibiotics clinically, will be degraded rapidly in natural habitats once released into the environment.

Biological Activities of the Nanoantibiotics before and after Degradation by Cellulolysis. Both the GPC and the viscosity studies confirmed that while the nanostructured PMBs maintain their structural integrity in the absence of cellulases, they are shredded into small pieces in the presence of the enzymes. Since cellulases do not exist in the human body but are ubiquitous in natural habitats, our data illustrate a

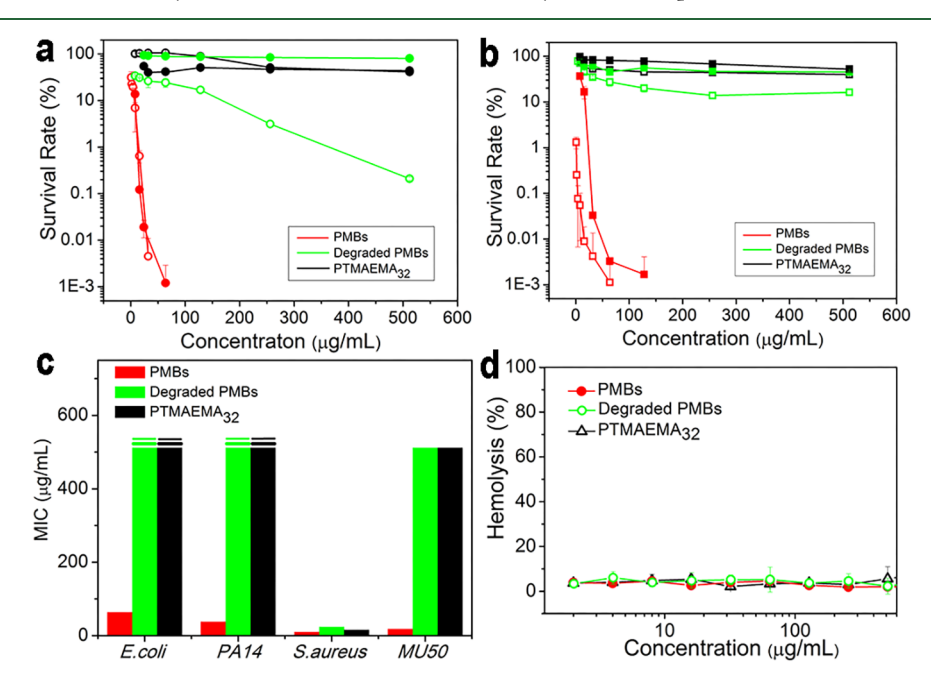


Figure 3. Comparison of the biological activities of PMBs, degraded PMBs, and linear-chain PTMAEMA<sub>32</sub> control. Bacterial killing assays against (a) Gram-negative *E. coli* (empty circle) and Gram-positive *S. aureus* (solid circle) as well as (b) clinical drug-resistant strains, i.e., Gram-negative *PA14* (empty square) and Gram-positive *MUS0* (solid square) show that while the nanostructured PMBs are potent killers for all bacteria, the degraded PMBs and linear-chain brush polymer control are ineffective bactericides. (c) Bacterial inhibitory assays also corroborate the same trend, i.e., while nanostructure gives rise to the bacterial inhibitory potency of PMBs, cellulase degradation annihilates this acquired potency and reduces it to the same level as that of the linear-chain brush polymer control. (d) Hemolysis assays against HRBCs show that all of the hydrophilic polymers are nonhemolytic.

Table 1. Summary of the Biological Activities PMBs, Degraded PMBs, and PTMAEMA<sub>32</sub>

	MBC ( $\mu$ g/mL)				MIC $(\mu g/mL)$				$HC_{50}$
	E.C. <sup>a</sup>	PA14	S.A. <sup>b</sup>	MU50	E.C.	PA14	S.A.	MU50	HRBC
PMBs	32	4	24	32	64	38	10	18	no <sup>c</sup>
degraded PMBs	no	no	no	no	no	no	24	512	no
$PTMAEMA_{32}$	no	no	no	no	no	no	16	512	no
<sup>a</sup> E. coli. <sup>b</sup> S. aureus. <sup>c</sup> Not obtained up to 512 μg/mL.									

unique *environmental* degradability of PMBs that differs from the in vivo biodegradability reported before<sup>22–25</sup> and suggest a new concept of mitigating the environmental footprints of antibiotics with rationally designed nanoantibiotics that can be dismantled and disabled by bioorthogonal chemistry occurring exclusively in natural habitats.

To illustrate this concept, we measured the biological activities of model PMBs before and after cellulase degradation and compared that with the linear-chain PTMAEMA<sub>32</sub> control (Figure 3). We used standard bacteria killing and inhibitory assays<sup>30,52,53</sup> against two representative strains from each bacterial family, i.e., Gram-negative E. coli and PA14 and Gram-positive S. aureus and MU50, respectively, in which the PA14 (i.e., tobramycin- and gentamycin-resistant P. aeruginosa) and MU50 (i.e., methicillin-, oxacillin-, and vancomycinresistant S. aureus) are clinical multidrug-resistant bacterial strains. We also tested the toxicity of all polymers by standard hemolysis and hemagglutination assays against HRBCs to obtain their respective HC<sub>50</sub> (i.e., the antibiotic concentration at which 50% of the HRBCs are lysed). 30,49,54 A list of HC50, minimum bactericidal concentration (MBC) and bacterial inhibitory concentration (MIC) of the PMBs, degraded PMBs, and linear-chain brush polymer control are compared in Table

Consistent with previous reports, 43,48,49 the hydrophilic linear-chain PTMAEMA brush by itself is nonhemolytic (Figure 3d) but antimicrobially inactive (Figure 3a-c). Cytotoxicity assays showed that it displays no cytotoxicity to HEK-293 cells (Figures S9 and S10, Supporting Information), but like many other cationic polymers, 55,56 it induces severe hemagglutination of HRBCs (Figure S8, Supporting Information). Surprisingly, while covalent assembly of the hydrophilic and antimicrobially inactive PTMAEMA brushes into nanostructured PMBs does not change their nonhemolytic nature (Figure 3d) or noncytotoxic property with HEK-293 cells (Figures S9 and S10, Supporting Information), it evokes a fundamental transition that completely eases their hemagglutination propensity (Figure S8, Supporting Information) and turns the PMBs into potent antimicrobials (Figure 3a-c). Bacterial killing assays against E. coli and S. aureus (Figure 3a) or against the multidrug-resistant PA14 and MU50 (Figure 3b) clearly showed that while the linear-chain brush polymer control itself exhibits negligible bactericidal activity, the nanostructured PMBs are turned into potent bacteria killers with MBCs ranging from 4 to 32  $\mu$ g/mL (Table 1). This nanostructure-associated transformation of hemagglutination behavior (Figure S8, Supporting Information) and antimicrobial activity (Figure 3a-c) resembles that reported before<sup>30</sup> but has an important difference: unlike previously reported PMBs with well-defined nanostructures that displayed a sizedependent selectivity between Gram-negative and Grampositive bacteria, 30 the cellulose-based PMBs kill both Gramnegative and Gram-positive bacteria with comparable potency (Figure 3a and 3b; Table 1). We confirmed that this difference

is due to the polydisperse nature of cellulose-based PMBs rather than their different brush chemistry, because the same size-dependent selectivity did show up nicely for PTMEAMA brushes grown on well-defined polymer backbones instead of the polydisperse cellulose (Figures S6 and S7, Supporting Information).

The nanostructure-dependent transformation of hemagglutination behavior and antimicrobial activity is further demonstrated by the observation that the acquired hemagglutination deficiency and antimicrobial potency of PMBs were lost once their nanostructure fell apart. Enzymatic degradation by cellulases for 3 h dismantled PMBs (Figure 2b), which in turn reactivated their hemagglutination propensity (Figure S8, Supporting Information) and eradicated their bactericidal activity, and no MBC was reached for the degraded PMBs against all bacterial strains up to 512  $\mu$ g/mL (Figure 3a and 3b; Table 1). The bacterial inhibitory assays followed the same suit (Figure 3c; Table 1): while the nanostructured PMBs are strongly bacteriostatic to all bacteria, cellulase degradation decimated the acquired potency and returned it to a similar level as that of the linear-chain brush polymer control. Notice that the MICs of degraded PMBs and linear-chain brush polymer against S. aureus is only slightly higher than that of the PMBs, which is consistent with previous reports that cationic compounds are in general strongly bacteriostatic against S. aureus, 57,58 but a significant difference between the two camps was observed against the multidrug-resistant MU50, demonstrating again the collective transformation of the antimicrobial activity of hydrophilic polymers once assembled into distinct nanostructures. Clearly, assembly and disassembly of the hydrophilic nanostructure is a two-way switch that turns on and off the acquired hemagglutination deficiency and antimicrobial activity.

Nanostructure Is Key for Hydrophilic Polymers to Disrupt Bacterial Membranes. Given that the primary difference setting the PMBs apart from degraded PMBs and linear-chain brush polymer control is the nanostructure of PMBs, the observed transformation of hemagglutination and bactericidal activities underscores their different modes of interactions with HRBCs or bacteria that depend critically on the nanostructure. In contrast to amphiphilic antimicrobial peptides and their synthetic mimics that can disrupt both bacterial and mammalian cell membranes impartially via hydrophobic interactions, <sup>59–62</sup> the PMBs, degraded PMBs, and linear-chain brush polymer are all hydrophilic and do not intercalate into the hydrophobic cell membrane interior. While the reason for the nanostructure-associated transformation of hemagglutination propensity is unknown and still under further investigation, our previous study showed that hydrophilic spherical or rod-like PMBs with well-defined nanostructures induced a topological transition exclusively on bacterial membranes to form pores while their linear-chain brush polymers did not.<sup>30</sup> This unique mode of membrane disruption had nothing to do with hydrophobic interactions.

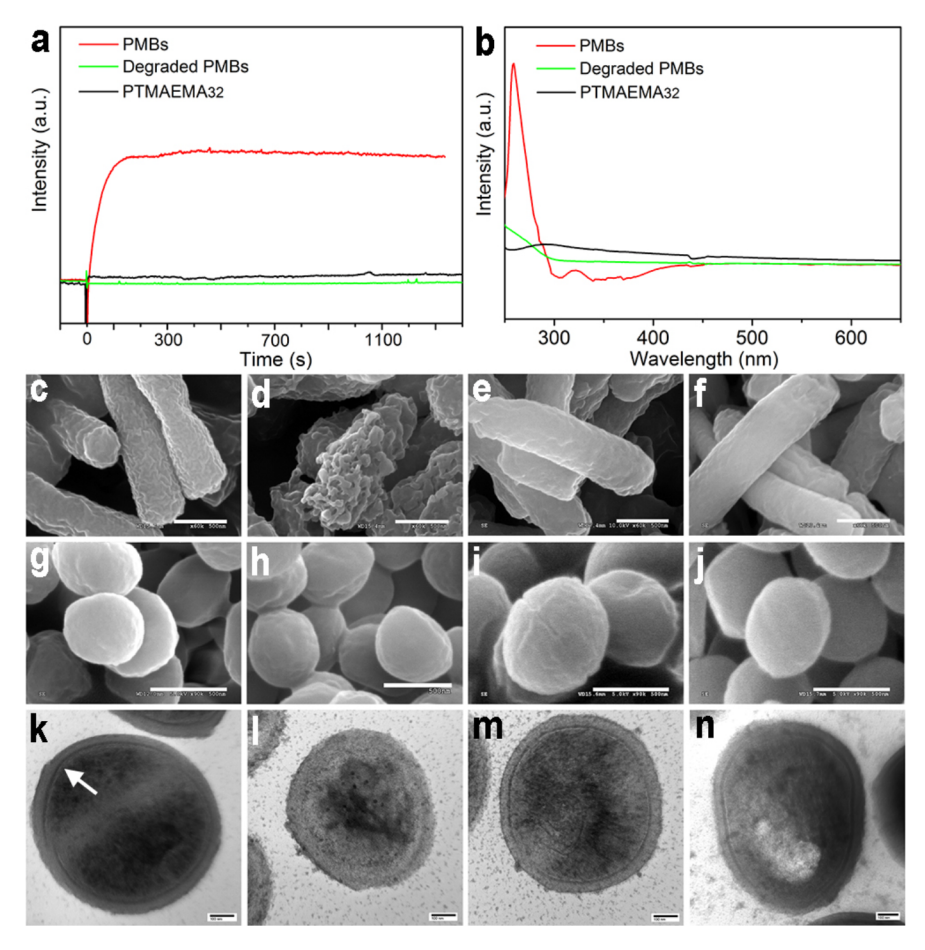


**Figure 4.** Different modes of interactions between hydrophilic PMBs, degraded PMBs, and linear-chain brush polymer against bacterial membranes hinge on the nanostructure. Membrane permeability (a) and cytoplasmic release assays (b) against *E. coli* show that only PMBs disrupt the bacterial membrane. SEM pictures (scale bar 500 nm) of *E. coli* (c-f) and *S. aureus* (g-j) by themselves (c, g) or treated by PMBs (d, h), degraded PMBs (e, i), and linear-chain PTMAEMA<sub>32</sub> (f, j) reveal that for the Gram-negative *E. coli*, only PMBs rupture the bacterial membrane by inducing radical topological changes (d). For the Gram-positive *S. aureus*, although no obvious morphological difference between untreated (g) and treated bacteria (h-j) is observed under SEM, cross-sectional TEM (scale bar 100 nm) clearly shows that only PMBs disrupt the bacterial membrane: in contrast to untreated *S. aureus* (k) and that treated by degraded PMBs (m) or linear-chain PTMAEMA<sub>32</sub> (n), where intact bacterial plasma membrane underneath the peptidoglycan encapsulation layer is discernible (stained by OsO<sub>4</sub> and marked by a white arrow in k), the plasma membrane of PMB-treated *S. aureus* (l) is obliterated out of existence.

Rather, it was attributed to two synergistic actions: (1) the strong multivalent interactions between hydrophilic PMBs and bacterial membranes that favor membrane wrapping around the nanostructured PMBs instead of linear-chain polymers and (2) the negative intrinsic curvature lipids rich in microbial membranes that further help offset the energy cost to bend the bacterial instead of mammalian membranes collectively around these nanostructures. Since this mode of action does not call on specific nanostructures, we anticipate that the cellulose-based PMBs, despite their polydisperse nanorod lengths, would also disrupt bacterial membranes following the same mechanism, while the degraded PMBs or linear-chain brush polymer would not due to the lack of distinct nanostructures and the nanostructure-associated multivalent interactions with bacterial membranes.

To test the critical role of nanostructures on bacterial membrane disruptions, we performed the membrane permeability assay for *E. coli* treated by PMBs, degraded PMBs, and linear-chain brush polymer control using fluorescent probe 1-*N*-phenylnaphthylamine (NPN), as permeation of the hydrophobic NPN into disrupted outer membranes of Gramnegative bacteria causes a prominent increase of its fluorescent

emission.<sup>63</sup> We also conducted the cytoplasmic release assay to monitor the leach of nucleic acids when bacterial membrane is compromised.<sup>64</sup> Both the membrane permeability and the cytoplasmic release assays showed that only nanostructured PMBs disrupted the *E. coli* membrane. As an example, increased NPN fluorescence emission at 420 nm and nucleic acid absorbance at 260 nm show up only for PMB-treated *E. coli* cells but not for those treated by degraded PMBs or linear-chain brush polymer control (Figure 4a and 4b).

This nanostructure-dependent membrane disruption is also on display under SEM: while untreated *E. coli* (Figure 4c) and those treated by degraded PMBs ((Figure 4e) or linear-chain brush polymer PTMAEMA<sub>32</sub> (Figure 4f) show uncompromised membrane morphology, those treated by PMBs (Figure 4d) are crumbled. For Gram-positive *S. aureus* cells that have a thick peptidoglycan layer encapsulating their membranes, no obvious difference is observed under SEM between untreated bacteria (Figure 4g) and those treated by PMBs (Figure 4h), degraded PMBs (Figure 4i), or linear-chain PTMAEMA<sub>32</sub> (Figure 4j). However, cross-sectional TEM clearly reveals obliteration of the *S. aureus* membrane beneath its peptidoglycan encapsulation layer after interaction with

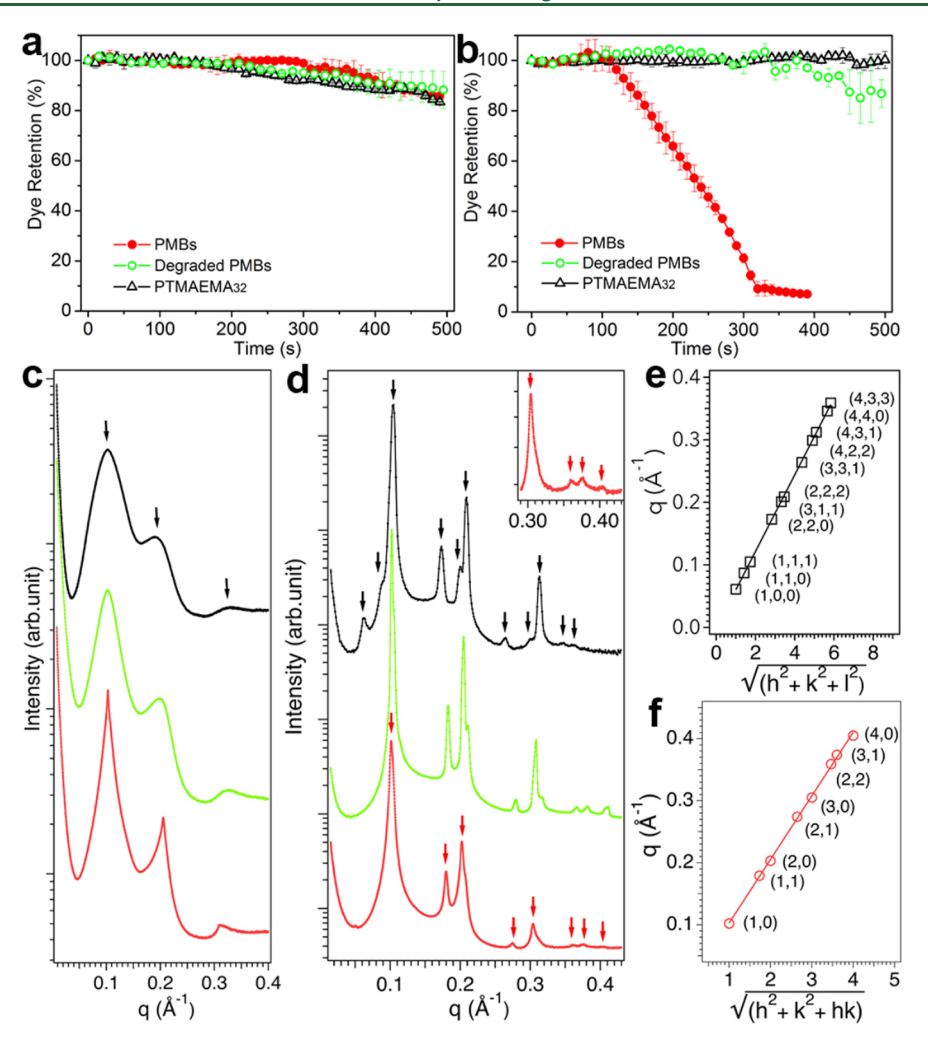


Figure 5. Structural evolution of model liposomes treated by hydrophilic polymers with dismantling nanostructures from PMBs to degraded PMBs and linear-chain brush polymer. Confocal microscopy of fluorescein-loaded GUVs that mimic mammalian cell and bacteria reveals that no dye leakage occurs when the mammalian cell-mimicking GUVs are treated by any hydrophilic polymer (a), while the same is only true for bacteria-mimicking GUVs treated by degraded PMBs or linear-chain brush polymer but not by PMBs (b). SAXS of (c) mammalian cell-mimicking and (d) bacteria-mimicking liposomes incubated with individual polymers (color scheme is the same as that in a and b) reveals different patterns on membrane remodeling that depend on both the membrane lipid composition and the polymer nanostructure: while the mammalian-mimicking membrane simply adheres to hydrophilic polymers to form a loosely bound membrane—polymer multilamellar structure without compromising the membrane integrity (c), the bacteria-mimicking membrane undergoes topological changes in response to different polymers to assume different remodeled structures (d), from a 2D hexagonal phase for the nanostructured PMBs (f) to a 3D cubic phase for the degraded PMBs and linear-chain brush polymer (e). (Inset in d) Blown-out view of the SAXS (0.29–0.43 Å<sup>-1</sup>) of bacteria-mimicking liposomes remodeled by PMBs.

PMBs (Figure 4l), in sharp contrast to the intact membrane of untreated *S. aureus* (Figure 4k) and those treated by degraded PMBs (Figure 4m) or linear-chain PTMAEMA<sub>32</sub> (Figure 4n).

Mechanistic Insights on Nanostructure as a Two-Way Switch to Turn ON/OFF the Membrane-Active Activities of Hydrophilic Polymers against Bacteria Instead of Mammalian Cells. Although none of the hydrophilic polymers disrupt the HRBC membrane (Figure 3d) or kill the HEK-293 cells (Figures S9 and S10, Supporting Information), bacteria are subjected to membrane disruption selectively by the nanostructured PMBs while spared by degraded PMBs and linear-chain brush polymer control (Figures 4 and 3a-c). The different disruptive actions of the PMBs, degraded PMBs, and linear-chain brush polymer control against bacterial and mammalian membranes underline a cooperative membrane remodeling mechanism that depends on both the membrane type and the polymer nanostructure. An important difference between mammalian and microbial

membranes is their lipid compositions. 65-68 Unlike mammalian membranes that predominantly consist of lipids with zero intrinsic curvature, microbial membranes are laden with lipids of negative intrinsic curvatures. To illustrate how membrane intrinsic curvature helps define the cooperative remodeling of biomembranes by the hydrophilic polymers, we monitored the structural evolution of model liposomes consisting of lipids with different intrinsic curvatures incubated with polymers of dismantling nanostructures, from PMBs to degraded PMBs and linear-chain brush polymer control, using confocal microscopy and SAXS, respectively (Figure 5). The model liposomes consist of mixtures of anionic lipid DOPG with zwitterionic DOPC and DOPE. Both DOPG and DOPC have zero intrinsic curvature, whereas DOPE has a negative intrinsic curvature. Following the pioneering works by Wong and colleagues that demonstrated successfully the utility of model membranes for understanding the action modes of membraneactive antimicrobials, <sup>69,70</sup> we used 20/80 (molar ratio)

DOPG/DOPE and DOPG/DOPC to mimic the PE-rich bacterial and PC-rich mammalian membranes, respectively, by keeping the membrane charge density the same.

We first probed the membrane disruption of mammalian cell- and bacteria-mimicking GUVs treated by each hydrophilic polymer by loading the GUVs with a fluorescent dye (i.e., fluorescein) and using confocal microscopy to monitor the dye leakage from individual GUVs. For the mammalian cellmimicking GUVs, no dye leakage was observed after interacting with any polymer (Figure 5a), suggesting none of the hydrophilic polymers disrupted the mammalian-mimicking membrane, which is in line with what was observed in the hemolysis (Figure 3d) and cytotoxicity assays (Figures S9 and S10, Supporting Information). For the bacteria-mimicking GUVs, although no membrane disruption was also observed for the degraded PMBs and linear-chain PTMAEMA<sub>32</sub> control, dye leakage did occur shortly after incubation with nanostructured PMBs, again resonating with earlier SEM observations that only the nanostructured PMBs were able to rupture bacterial membranes (Figure 4). Despite its limitations,<sup>71</sup> the dye leakage experiment highlights the importance of both the intrinsic curvature of membrane lipids and polymer nanostructure on how hydrophilic polymers remodel biomembranes: while the mammalian-mimicking membranes rich in lipids of zero intrinsic curvature resist disruptions against all hydrophilic polymers, the bacteria-mimicking membranes rich in lipids of negative intrinsic curvature only resist disruptions against degraded PMBs or linear-chain brush polymer control but are liable to rupture in the presence of nanostructured PMBs. Dismantling the nanostructure effectively turns off the membrane disruption activity of the PMBs.

To gain mechanistic insight about the structural evolution of biomembranes that gives rise to the different dye leakage behaviors, we used SAXS to identify the coassembled phases of mammalian cell- and bacteria-mimicking liposomes incubated with each hydrophilic polymer. The unilamellar liposomes by themselves show a weak and broad SAXS peak characteristic of the liposome form factor. <sup>69,72</sup> After interacting with individual hydrophilic polymers, three broad harmonics characteristic of a loosely bound multilamellar structure showed up for the mammalian cell-mimicking liposomes (Figure 5c, marked by black arrows) with the first peak  $(q_{001})$  centered around 0.102  $Å^{-1}$ , indicating a lamellar periodicity of  $\sim$ 62 Å. We attributed this coassembled phase as alternating lipid and polymer layers loosely coupled to each other due to attractive electrostatic interactions, confirming that the membrane rich in lipids of zero intrinsic curvature maintains its structural integrity after interacting with the hydrophilic polymers.

When the membrane charge density was kept the same (i.e., 20% anionic DOPG) but the zero intrinsic curvature lipid DOPC was replaced by the negative intrinsic curvature lipid DOPE to mimic microbial membranes, we observed completely different membrane remodeling behaviors before and after the polymer nanostructures fell apart (Figure 5d). For the membrane treated by nanostructured PMBs, a series of scattering peaks (marked by red arrows) at 0.102, 0.179, 0.203, 0.274, 0.305, 0.359, 0.374, and 0.405 Å<sup>-1</sup> showed up, which can be best fit as the first 8 reflections, i.e., (1,0), (1,1), (2,0), (2,1), (3,0), (2,2), (3,1), and (4,0), respectively, of a 2D hexagonal phase (Figure 5f). For the membrane treated by linear-chain brush polymer, a total of 11 reflections (marked by black arrows) at 0.061, 0.087, 0.105, 0.173, 0.201, 0.209, 0.264,

0.299, 0.313, 0.346, and 0.359  $\mbox{\normalfont\AA}^{-1}$  showed up. Those peaks have a relationship of

1: 
$$\sqrt{2}$$
:  $\sqrt{3}$ :  $\sqrt{8}$ :  $\sqrt{11}$ :  $\sqrt{12}$ :  $\sqrt{19}$ :  $\sqrt{24}$ :  $\sqrt{26}$ :  $\sqrt{32}$ :  $\sqrt{35}$ 

and fit nicely as the (1,0,0), (1,1,0), (1,1,1), (2,2,0), (3,1,1), (2,2,2), (3,3,1), (4,2,2), (4,3,1), (4,4,0), and (5,3,1) reflections, respectively (Figure 5e), of a 3D cubic phase (e.g., Pm3m) with a lattice parameter of 103 Å. In between the two ends of the spectrum sits the membrane treated by degraded PMBs (Figure 5d, green trace); its scattering peaks are positioned at 0.102, 0.183, 0.205, 0.211, 0.279, 0.308, 0.317, 0.365, 0.382, and 0.409 Å<sup>-1</sup>, respectively. These peaks are related to each other by the ratio of

$$\sqrt{3}$$
:  $\sqrt{10}$ :  $\sqrt{12}$ :  $\sqrt{13}$ :  $\sqrt{22}$ :  $\sqrt{27}$ :  $\sqrt{29}$ :  $\sqrt{38}$ :  $\sqrt{42}$ :  $\sqrt{48}$ 

which again can be identified as the (1,1,1), (3,1,0), (2,2,2), (3,2,0), (3,3,2), (3,3,3), (4,3,2), (5,3,2), (5,4,1), and (4,4,4) reflections, respectively, of a 3D cubic phase (e.g., Pm3m or P432) with a slightly different lattice parameter of 107 Å. The structural evolution revealed by SAXS clearly illustrates the different modes of actions between the bacteria-mimicking membrane and the hydrophilic polymers that hinge on the polymer nanostructure. The rod-like PMBs, despite their polydisperse nanorod lengths, are able to transform the bacteria-mimicking membrane into a simple 2D hexagonal structure. Enzymatic degradation of PMBs abolishes this unique capability; both the dismantled PMBs and the linearchain brush polymer control interact with the membrane in a different way that favors formation of a 3D cubic phase. Since only the PMBs act as the membrane-active nanoantibiotics that kill bacteria (Figures 3 and 4), we reason that the remodeling of the bacterial membrane by the hydrophilic polymers into a 2D hexagonal phase rather than a 3D cubic phase sets the irreversible process of membrane disruption.

To further understand the critical role of this 2D hexagonal phase on bacterial membrane disruption, we performed Fourier reconstruction of the PMB-remodeled bacteria-mimicking membrane using the method reported before. 30,69,73 On the basis of the phase criteria developed by Turner and Gruner, 73 our phase choices are (+--+++++). The reconstructed electron density map along the membrane plane clearly reveals the 2D hexagonally packed membrane pores (Figure 6a).

Close examination of the 1D electron density profile along the axis of the hexagonal lattice (Figure 6b) further helps identify the molecular details on how the membrane pores are formed. The region in between the pores has the lowest electron density ( $\rho = 0.29 \text{ e/Å}^3$ ), which is attributed to the hydrocarbon lipid tails. Approaching the rim of those pores, the electron density rises to 0.55 e/Å<sup>3</sup>. It then drops to 0.43 e/ Å<sup>3</sup> inside the pores before a rod-like feature appears at the center of the pores with the highest electron density ( $\rho = 0.66$ e/Å<sup>3</sup>). This rod-like feature can be only assigned to PMB because only the PMBs have high-electron-density iodide counterions associated with their PTMAEMA brushes. Accordingly, the second highest electron density at the rim  $(\rho = 0.55 \text{ e/Å}^3)$  can be only assigned to phospholipid headgroups because they are the only candidates with the next highest electron density after PMBs. The reconstructed electron density at the rim is higher than that of a typical phospholipid headgroup (0.41 e/ų), suggesting the presence of residue iodide ions. The presence of residue iodide ions is further confirmed by the increased electron density inside the

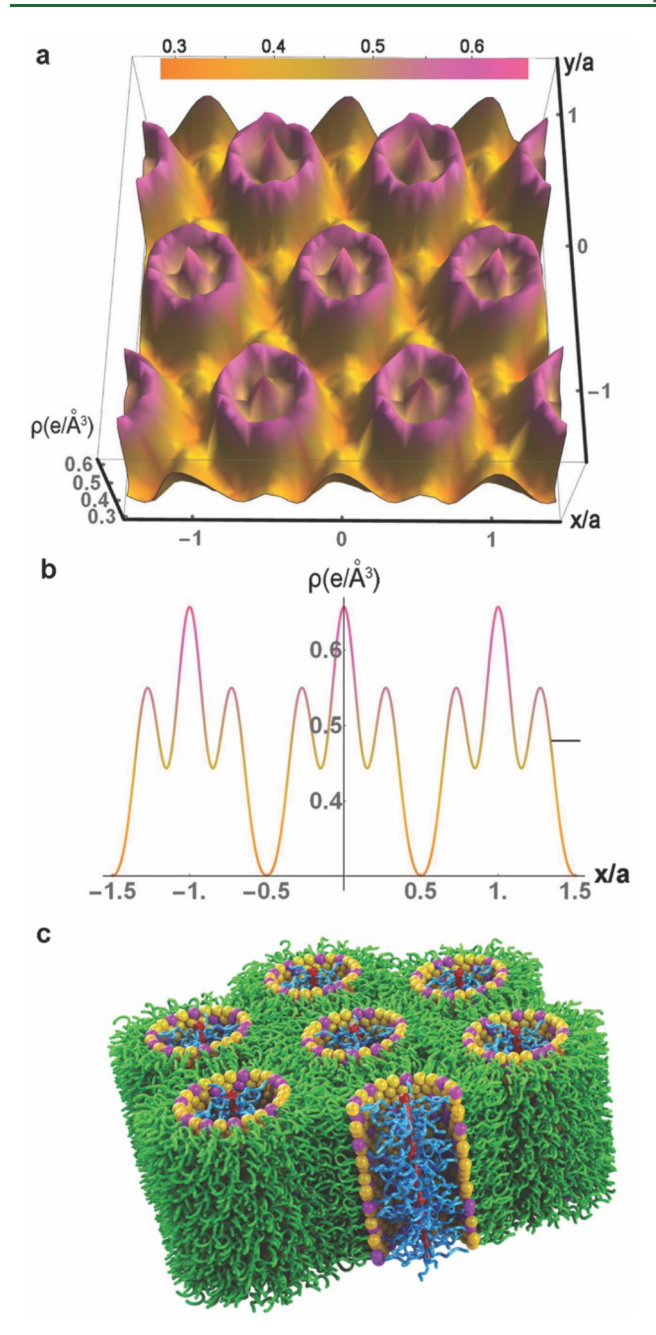


Figure 6. Fourier reconstruction reveals that nanostructured PMBs remodel bacteria-mimicking membrane by inducing a topological transition to form membrane pores. (a) Reconstructed electron density map of remodeled bacteria-mimicking membrane clearly displays the 2D hexagonally packed membrane pores. Scale bar of electron density  $(\rho)$  is shown at the top, and x/a and y/a represent perpendicular axes along the membrane plane normalized by the lattice parameter. (b) One-dimensional electron density profile along the x axis of the remodeled membrane plane further identifies how the PMBs induce topological transition of membranes to form pores: individual rod-like PMBs ( $\rho = 0.66 \text{ e/Å}^3$ ) located at the center of each pore are wrapped around by a wall of lipid headgroups ( $\rho = 0.55 \text{ e/}$ Å<sup>3</sup>) with the hydrocarbon tails ( $\rho = 0.29 \text{ e/Å}^3$ ) of those lipids distributed radially in between the pores to form a 2D inverted hexagonal phase  $(H_{II})$ . (c) Schematic illustration of the reconstructed nanoporous membranes remodeled by PMBs (blue and red, PTMAEMA brushes and cellulose backbone of the rod-like PMBs, respectively; gold, DOPG headgroup; magenta, DOPE headgroup; green, lipid tails).

aqueous pores ( $\rho$  = 0.43 e/ų), which is much higher than water by itself ( $\rho$  = 0.33 e/ų).³0,73

On the basis of the Fourier reconstruction, a schematic illustration of the PMB-remodeled membrane is built (Figure 6c). This honeycomb-like 2D inverted hexagonal phase  $(H_{II})$  is the hallmark of membrane pore formation and likely the root cause of bacteria death because the loss of homeostasis would set the irreversible process of membrane disruption. The nanostructure of hydrophilic rod-like PMBs is instrumental to their antimicrobial activities, because only the nanostructured PMBs give rise to multivalent interactions that induce a topological transition of bacterial membranes to wrap around the nanostructures to form pores. The multivalent interactions are lost when the same nanostructures fall apart due to enzymatic degradation and so is the acquired antimicrobial potency (Figure 3). In addition, this nanostructure-dependent membrane disruption only applies to bacterial membranes rich in lipids of negative intrinsic curvature, because the negative intrinsic curvature helps offset the energy cost to bend the bacterial membrane collectively around the nanostructures. No topological transition or membrane disruption occurs when the negative intrinsic curvature lipids are replaced with zero intrinsic curvature lipids to mimic mammalian membranes (Figures 4 and 5), because the energy cost to bend those membranes toward pore formation would be prohibitively high.

#### CONCLUSIONS

In summary, we demonstrated that assembly of the hydrophilic and antimicrobially inactive linear-chain polymers into nanostructured PMBs turns "ON" their antimicrobial activities collectively, while disassembly of the nanostructured PMBs turns the acquired activities "OFF". The nanostructure itself is the linchpin of this transformation, and cellulase degradation epitomizes the bioorthogonal chemistry that acts as an environment-specific switch to deactivate the antimicrobial activities of nanoantibiotics. We elucidated that the root cause of the antimicrobial activities of hydrophilic polymers is the nanostructure-induced topological change of the bacterial membrane that results in pore formation, and this two-way switch of membrane disruption works exclusively on bacterial membranes laden with lipids of negative intrinsic curvature, because negative membrane curvature is needed to help offset the energy cost to bend the membrane collectively around the nanostructured PMBs. The hydrophilic nanostructures wreak havoc to bacterial membranes yet remain inactive against mammalian membranes rich in lipids of zero intrinsic curvature. Our study illuminates a new concept of modular nanoantibiotic design to mitigate the environmental footprints of antibiotics: (1) "plug-to-activate": hydrophilic, nontoxic, and antimicrobially inactive molecules can be transformed into potent antibiotics once assembled into supramolecular nanostructures; (2) "unplug-to-deactivate": with the built-in disassembly switches responsive to bioorthogonal stimuli occurring exclusively in natural habitats, these nanoantibiotics will remain fully active while in clinical services but fall apart and become antimicrobially inactive pieces once released into the environment.

## ■ ASSOCIATED CONTENT

#### **Supporting Information**

The Supporting Information is available free of charge at https://pubs.acs.org/doi/10.1021/acs.biomac.0c00163.

Experimental details on the synthesis and characterization of model PMBs and linear-chain brush polymer control, as well as results of hemagglutination and cytotoxicity assays (PDF)

### AUTHOR INFORMATION

#### **Corresponding Author**

Hongjun Liang — Department of Cell Physiology & Molecular Biophysics, Texas Tech University Health Sciences Center, Lubbock, Texas 79430, United States; Department of Chemical Engineering and Department of Chemistry, Texas Tech University, Lubbock, Texas 79409, United States; oorcid.org/0000-0003-0864-9106; Email: H.liang@ttuhsc.edu

#### **Authors**

Wan Zheng – Department of Cell Physiology & Molecular Biophysics, Texas Tech University Health Sciences Center, Lubbock, Texas 79430, United States; orcid.org/0000-0002-5475-5340

**Miguel Anzaldua** – Department of Chemical Engineering, Texas Tech University, Lubbock, Texas 79409, United States

Ankita Arora — Department of Cell Physiology & Molecular Biophysics, Texas Tech University Health Sciences Center, Lubbock, Texas 79430, United States; Department of Materials Science and Engineering, Indian Institute of Technology Gandhinagar, Gujarat 382355, India

Yunjiang Jiang — Department of Cell Physiology & Molecular Biophysics, Texas Tech University Health Sciences Center, Lubbock, Texas 79430, United States

Kelly McIntyre – Department of Cell Physiology & Molecular Biophysics, Texas Tech University Health Sciences Center, Lubbock, Texas 79430, United States

Michael Doerfert – Department of Chemical Engineering, Texas Tech University, Lubbock, Texas 79409, United States

**Theodora Winter** – The Honors College, Texas Tech University, Lubbock, Texas 79409, United States

Abhijit Mishra — Department of Materials Science and Engineering, Indian Institute of Technology Gandhinagar, Gujarat 382355, India; o orcid.org/0000-0003-1057-3550

Hairong Ma – Department of Cell Physiology & Molecular Biophysics, Texas Tech University Health Sciences Center, Lubbock, Texas 79430, United States

Complete contact information is available at: https://pubs.acs.org/10.1021/acs.biomac.0c00163

#### **Author Contributions**

The manuscript was written through contributions of all authors. All authors have given approval to the final version of the manuscript.

#### **Notes**

The authors declare no competing financial interest.

#### ACKNOWLEDGMENTS

This work was supported in part by the NSF through DMR-1810767, the South Plains Foundation, and the CH Foundation. We thank Prof. Kendra Rumbaugh for providing the clinical multidrug-resistant *PA14* and *MU50* strains and Prof. Min Kang for providing the HEK-293 cells. A.A. and A.M. acknowledge the Overseas Research Exposure Fellowship funded by the Indian Institute of Technology (IIT) Gandhinagar. Synchrotron SAXS experiments were performed

at SSRL, which is supported by the DOE Office of Basic Energy Sciences under Contract No. DE-AC02-76SF00515.

#### ABBREVIATIONS

PMB, polymer molecular brush; DP, degree of polymerization; ATRP, atom transfer radical polymerization; AMIMCl, 1-allyl-3-methylimidazolium chloride; PDMAEMA, poly(N,N-dimethylamino-2-ethyl methacrylate); PTMAEMA, poly(N,N,N-trimethylamino-2-ethyl methacrylate); DOPG, 1,2-dioleoyl-sn-glycero-3-phospho-(1'-rac-glycerol) (sodium salt); DOPC, 1,2-dioleoyl-sn-glycero-3-phosphocholine; DOPE, 1,2-dioleoyl-sn-glycero-3-phosphocholine; HRBC, human red blood cell; NPN, 1-N-phenylnaphthylamine; MBC, minimum bactericidal concentration; MIC, minimum bacteria inhibitory concentration; SAXS, small-angle X-ray scattering; SEM, scanning electron microscopy; TEM, transmission electron microscopy; GPC, gel permeation chromatography; NMR, nuclear magnetic resonance; FTIR, Fourier transform infrared spectroscopy

#### REFERENCES

- (1) Du, L. F.; Liu, W. K. Occurrence, fate, and ecotoxicity of antibiotics in agro-ecosystems. A review. *Agron. Sustainable Dev.* **2012**, 32 (2), 309–327.
- (2) Finley, R. L.; Collignon, P.; Larsson, D. G. J.; McEwen, S. A.; Li, X. Z.; Gaze, W. H.; Reid-Smith, R.; Timinouni, M.; Graham, D. W.; Topp, E. The Scourge of Antibiotic Resistance: The Important Role of the Environment. *Clin. Infect. Dis.* **2013**, *57* (5), 704–710.
- (3) Kemper, N. Veterinary antibiotics in the aquatic and terrestrial environment. *Ecol. Indic.* **2008**, *8* (1), 1–13.
- (4) Spielmeyer, A.; Hoper, H.; Hamscher, G. Long-term monitoring of sulfonamide leaching from manure amended soil into groundwater. *Chemosphere* **2017**, *177*, 232–238.
- (5) Pan, M.; Chu, L. M. Adsorption and degradation of five selected antibiotics in agricultural soil. *Sci. Total Environ.* **2016**, *545*, 48–56.
- (6) Liu, X. H.; Lu, S. Y.; Guo, W.; Xi, B. D.; Wang, W. L. Antibiotics in the aquatic environments: A review of lakes, China. *Sci. Total Environ.* **2018**, *627*, 1195–1208.
- (7) Faleye, A. C.; Adegoke, A. A.; Ramluckan, K.; Bux, F.; Stenstrom, T. A. Antibiotic Residue in the Aquatic Environment: Status in Africa. *Open Chem.* **2018**, *16* (1), 890–903.
- (8) Carvalho, I. T.; Santos, L. Antibiotics in the aquatic environments: A review of the European scenario. *Environ. Int.* **2016**, *94*, 736–757.
- (9) Li, Y. W.; Wu, X. L.; Mo, C. H.; Tai, Y. P.; Huang, X. P.; Xiang, L. Investigation of Sulfonamide, Tetracycline, and Quinolone Antibiotics in Vegetable Farmland Soil in the Pearl River Delta Area, Southern China. *J. Agric. Food Chem.* **2011**, 59 (13), 7268–7276.
- (10) Kummerer, K. Antibiotics in the aquatic environment A review Part I. *Chemosphere* **2009**, *75* (4), 417–434.
- (11) Hammesfahr, U.; Heuer, H.; Manzke, B.; Smalla, K.; Thiele-Bruhn, S. Impact of the antibiotic sulfadiazine and pig manure on the microbial community structure in agricultural soils. *Soil Biol. Biochem.* **2008**, *40* (7), 1583–1591.
- (12) Grenni, P.; Ancona, V.; Barra Caracciolo, A. Ecological effects of antibiotics on natural ecosystems: A review. *Microchem. J.* **2018**, 136, 25–39.
- (13) Auguet, O.; Pijuan, M.; Borrego, C. M.; Rodriguez-Mozaz, S.; Triado-Margarit, X.; Della Giustina, S. V.; Gutierrez, O. Sewers as potential reservoirs of antibiotic resistance. *Sci. Total Environ.* **2017**, 605-606, 1047–1054.
- (14) Knapp, C. W.; Dolfing, J.; Ehlert, P. A. I.; Graham, D. W. Evidence of Increasing Antibiotic Resistance Gene Abundances in Archived Soils since 1940. *Environ. Sci. Technol.* **2010**, 44 (2), 580–587.

- (15) Gullberg, E.; Cao, S.; Berg, O. G.; Ilback, C.; Sandegren, L.; Hughes, D.; Andersson, D. I. Selection of Resistant Bacteria at Very Low Antibiotic Concentrations. *PLoS Pathog.* **2011**, *7* (7), No. e1002158.
- (16) Marti, E.; Variatza, E.; Balcazar, J. L. The role of aquatic ecosystems as reservoirs of antibiotic resistance. *Trends Microbiol.* **2014**, 22 (1), 36–41.
- (17) McBain, A. J.; Rickard, A. H.; Gilbert, P. Possible implications of biocide accumulation in the environment on the prevalence of bacterial antibiotic resistance. *J. Ind. Microbiol. Biotechnol.* **2002**, 29 (6), 326–330.
- (18) Kristiansson, E.; Fick, J.; Janzon, A.; Grabic, R.; Rutgersson, C.; Weijdegard, B.; Soderstrom, H.; Larsson, D. G. J. Pyrosequencing of Antibiotic-Contaminated River Sediments Reveals High Levels of Resistance and Gene Transfer Elements. *PLoS One* **2011**, *6* (2), No. e17038.
- (19) Andersson, D. I.; Hughes, D. Evolution of antibiotic resistance at non-lethal drug concentrations. *Drug Resist. Updates* **2012**, *15* (3), 162–172.
- (20) Blazquez, J.; Couce, A.; Rodriguez-Beltran, J.; Rodriguez-Rojas, A. Antimicrobials as promoters of genetic variation. *Curr. Opin. Microbiol.* **2012**, *15* (5), 561–569.
- (21) Wright, G. D. Antibiotic resistance in the environment: a link to the clinic? *Curr. Opin. Microbiol.* **2010**, *13* (5), 589–594.
- (22) Chin, W.; Yang, C. A.; Ng, V. W. L.; Huang, Y.; Cheng, J. C.; Tong, Y. W.; Coady, D. J.; Fan, W. M.; Hedrick, J. L.; Yang, Y. Y. Biodegradable Broad-Spectrum Antimicrobial Polycarbonates: Investigating the Role of Chemical Structure on Activity and Selectivity. *Macromolecules* 2013, 46 (22), 8797–8807.
- (23) Du, H.; Zha, G. Y.; Gao, L. L.; Wang, H.; Li, X. D.; Shen, Z. Q.; Zhu, W. P. Fully biodegradable antibacterial hydrogels via thiol-ene "click" chemistry. *Polym. Chem.* **2014**, *5* (13), 4002–4008.
- (24) Woo, G. L. Y.; Mittelman, M. W.; Santerre, J. P. Synthesis and characterization of a novel biodegradable antimicrobial polymer. *Biomaterials* **2000**, *21* (12), 1235–1246.
- (25) Qiao, Y.; Yang, C.; Coady, D. J.; Ong, Z. Y.; Hedrick, J. L.; Yang, Y. Y. Highly dynamic biodegradable micelles capable of lysing Gram-positive and Gram-negative bacterial membrane. *Biomaterials* **2012**, 33 (4), 1146–1153.
- (26) Pruden, A.; Larsson, D. G. J.; Amezquita, A.; Collignon, P.; Brandt, K. K.; Graham, D. W.; Lazorchak, J. M.; Suzuki, S.; Silley, P.; Snape, J. R.; Topp, E.; Zhang, T.; Zhu, Y. G. Management Options for Reducing the Release of Antibiotics and Antibiotic Resistance Genes to the Environment. *Environ. Health Perspect.* **2013**, *121* (8), 878–885.
- (27) Wang, B.; Lv, X. L.; Feng, D. W.; Xie, L. H.; Zhang, J.; Li, M.; Xie, Y. B.; Li, J. R.; Zhou, H. C. Highly Stable Zr(IV)-Based Metal-Organic Frameworks for the Detection and Removal of Antibiotics and Organic Explosives in Water. J. Am. Chem. Soc. 2016, 138 (19), 6204–6216.
- (28) Wen, X. J.; Niu, C. G.; Zhang, L.; Liang, C.; Guo, H.; Zeng, G. M. Photocatalytic degradation of ciprofloxacin by a novel Z-scheme  $CeO_2$ -Ag/AgBr photocatalyst: Influencing factors, possible degradation pathways, and mechanism insight. *J. Catal.* **2018**, 358, 141–154.
- (29) Xue, J. J.; Ma, S. S.; Zhou, Y. M.; Zhang, Z. W.; He, M. Facile Photochemical Synthesis of Au/Pt/g-C<sub>3</sub>N<sub>4</sub> with Plasmon-Enhanced Photocatalytic Activity for Antibiotic Degradation. *ACS Appl. Mater. Interfaces* **2015**, *7* (18), 9630–9637.
- (30) Jiang, Y. J.; Zheng, W.; Kuang, L. J.; Ma, H. R.; Liang, H. J. Hydrophilic Phage-Mimicking Membrane Active Antimicrobials Reveal Nanostructure-Dependent Activity and Selectivity. *ACS Infect. Dis.* **2017**, 3 (9), 676–687.
- (31) Zhang, H.; Wu, J.; Zhang, J.; He, J. 1-Allyl-3-methylimidazolium Chloride Room Temperature Ionic Liquid: A New and Powerful Nonderivatizing Solvent for Cellulose. *Macromolecules* **2005**, 38, 8272–8275.
- (32) Hua, D.; Jiang, J.; Kuang, L.; Jiang, J.; Zheng, W.; Liang, H. Smart Chitosan-Based Stimuli-Responsive Nanocarriers for the

- Controlled Delivery of Hydrophobic Pharmaceuticals. *Macromolecules* **2011**, *44*, 1298–1302.
- (33) Ghose, T. K. Measurement of cellulase activities. *Pure Appl. Chem.* 1987, 59 (2), 257–268.
- (34) Hasunuma, T.; Okazaki, F.; Okai, N.; Hara, K. Y.; Ishii, J.; Kondo, A. A review of enzymes and microbes for lignocellulosic biorefinery and the possibility of their application to consolidated bioprocessing technology. *Bioresour. Technol.* **2013**, *135*, 513–522.
- (35) King, B. C.; Waxman, K. D.; Nenni, N. V.; Walker, L. P.; Bergstrom, G. C.; Gibson, D. M. Arsenal of plant cell wall degrading enzymes reflects host preference among plant pathogenic fungi. *Biotechnol. Biofuels* **2011**, *4* (1), 4.
- (36) Wilson, D. B. Microbial diversity of cellulose hydrolysis. *Curr. Opin. Microbiol.* **2011**, *14* (3), 259–263.
- (37) Zhu, S. D.; Wu, Y. X.; Chen, Q. M.; Yu, Z. N.; Wang, C. W.; Jin, S. W.; Ding, Y. G.; Wu, G. Dissolution of cellulose with ionic liquids and its application: a mini-review. *Green Chem.* **2006**, 8 (4), 325–327.
- (38) Zhang, H.; Wu, J.; Zhang, J.; He, J. S. 1-Allyl-3-methylimidazolium chloride room temperature ionic liquid: A new and powerful nonderivatizing solvent for cellulose. *Macromolecules* **2005**, 38 (20), 8272–8277.
- (39) Kuang, L.; Goins, J.; Zheng, W.; Eduafo, P.; Ma, H.; Posewitz, M.; Wu, D. T.; Liang, H. Spontaneous Microalgae Dewatering Directed by Retrievable, Recyclable, and Reusable Nanoparticle-Pinched Polymer Brushes. *Chem. Mater.* **2019**, *31* (13), 4657–4672.
- (40) Zhang, Y.; Aigner, A.; Agarwal, S. Degradable and Biocompatible Poly(N,N-dimethylaminoethyl Methacrylate-co-caprolactone)s as DNA Transfection Agents. *Macromol. Biosci.* **2013**, *13* (9), 1267–1275.
- (41) Agarwal, S.; Zhang, Y.; Maji, S.; Greiner, A. PDMAEMA based gene delivery materials. *Mater. Today* **2012**, *15* (9), 388–393.
- (42) Car, A.; Baumann, P.; Duskey, J. T.; Chami, M.; Bruns, N.; Meier, W. pH-Responsive PDMS-*b*-PDMAEMA Micelles for Intracellular Anticancer Drug Delivery. *Biomacromolecules* **2014**, *15* (9), 3235–3245.
- (43) Rawlinson, L. A. B.; Ryan, S. M.; Mantovani, G.; Syrett, J. A.; Haddleton, D. M.; Brayden, D. J. Antibacterial Effects of Poly(2-(dimethylamino ethyl)methacrylate) against Selected Gram-Positive and Gram-Negative Bacteria. *Biomacromolecules* **2010**, *11* (2), 443–453.
- (44) Dong, H. C.; Huang, J. Y.; Koepsel, R. R.; Ye, P. L.; Russell, A. J.; Matyjaszewski, K. Recyclable Antibacterial Magnetic Nanoparticles Grafted with Quaternized Poly(2-(dimethylamino)ethyl methacrylate) Brushes. *Biomacromolecules* **2011**, *12* (4), 1305–1311.
- (45) Hancock, R. E. W.; Sahl, H. G. Antimicrobial and host-defense peptides as new anti-infective therapeutic strategies. *Nat. Biotechnol.* **2006**, 24 (12), 1551–1557.
- (46) Huang, H. W.; Charron, N. E. Understanding membrane-active antimicrobial peptides. *Q. Rev. Biophys.* **2017**, *50*, e10.
- (47) Sani, M. A.; Separovic, F. How Membrane-Active Peptides Get into Lipid Membranes. Acc. Chem. Res. 2016, 49 (6), 1130-1138.
- (48) Yancheva, E.; Paneva, D.; Maximova, V.; Mespouille, L.; Dubois, P.; Manolova, N.; Rashkov, I. Polyelectrolyte complexes between (cross-linked) N-carboxyethylchitosan and (quaternized) poly 2-(dimethylamino)ethyl methacrylate: Preparation, characterization, and antibacterial properties. *Biomacromolecules* **2007**, 8 (3), 976–984.
- (49) Palermo, E. F.; Kuroda, K. Chemical Structure of Cationic Groups in Amphiphilic Polymethacrylates Modulates the Antimicrobial and Hemolytic Activities. *Biomacromolecules* **2009**, *10* (6), 1416–1428.
- (50) Zhang, Y. H.; Lynd, L. R. Quantification of cell and cellulase mass concentrations during anaerobic cellulose fermentation: Development of an enzyme-linked immunosorbent assay-based method with application to Clostridium thermocellum batch cultures. *Anal. Chem.* **2003**, 75 (2), 219–227.

- (51) Pavel, R.; Doyle, J.; Steinberger, Y. Seasonal patterns of cellulase concentration in desert soil. *Soil Biol. Biochem.* **2004**, *36* (3), 549–554.
- (52) Wiegand, I.; Hilpert, K.; Hancock, R. E. W. Agar and broth dilution methods to determine the minimal inhibitory concentration (MIC) of antimicrobial substances. *Nat. Protoc.* **2008**, *3* (2), 163–175.
- (53) Andrews, J. M. Determination of minimum inhibitory concentrations. *J. Antimicrob. Chemother.* **2001**, *48*, 5–16.
- (54) Lienkamp, K.; Madkour, A. E.; Musante, A.; Nelson, C. F.; Nusslein, K.; Tew, G. N. Antimicrobial polymers prepared by ROMP with unprecedented selectivity: A molecular construction kit approach. J. Am. Chem. Soc. 2008, 130 (30), 9836–9843.
- (55) Samal, S. K.; Dash, M.; Van Vlierberghe, S.; Kaplan, D. L.; Chiellini, E.; van Blitterswijk, C.; Moroni, L.; Dubruel, P. Cationic polymers and their therapeutic potential. *Chem. Soc. Rev.* **2012**, *41* (21), 7147–7194.
- (56) Moreau, E.; Domurado, M.; Chapon, P.; Vert, M.; Domurado, D. Biocompatibility of polycations: In vitro agglutination and lysis of red blood cells and in vivo toxicity. *J. Drug Target.* **2002**, *10* (2), 161–173.
- (57) Furi, L.; Ciusa, M. L.; Knight, D.; Di Lorenzo, V.; Tocci, N.; Cirasola, D.; Aragones, L.; Coelho, J. R.; Freitas, A. T.; Marchi, E.; Moce, L.; Visa, P.; Northwood, J. B.; Viti, C.; Borghi, E.; Orefici, G.; Morrissey, I.; Oggioni, M. R.; Consortium, B. Evaluation of Reduced Susceptibility to Quaternary Ammonium Compounds and Bisbiguanides in Clinical Isolates and Laboratory-Generated Mutants of Staphylococcus aureus. *Antimicrob. Agents Chemother.* **2013**, *57* (8), 3488–3497.
- (58) Grare, M.; Dibama, H. M.; Lafosse, S.; Ribon, A.; Mourer, M.; Regnouf-de-Vains, J. B.; Finance, C.; Duval, R. E. Cationic compounds with activity against multidrug-resistant bacteria: interest of a new compound compared with two older antiseptics, hexamidine and chlorhexidine. *Clin. Microbiol. Infect.* **2010**, *16* (5), 432–438.
- (59) Scott, R. W.; DeGrado, W. F.; Tew, G. N. De novo designed synthetic mimics of antimicrobial peptides. Curr. Opin. Biotechnol. **2008**, 19 (6), 620–627.
- (60) Tew, G. N.; Scott, R. W.; Klein, M. L.; Degrado, W. F. De novo design of antimicrobial polymers, foldamers, and small molecules: From discovery to practical applications. *Acc. Chem. Res.* **2010**, 43 (1), 30–39.
- (61) Palermo, E. F.; Kuroda, K. Structural determinants of antimicrobial activity in polymers which mimic host defense peptides. *Appl. Microbiol. Biotechnol.* **2010**, *87* (5), 1605–1615.
- (62) Timofeeva, L.; Kleshcheva, N. Antimicrobial polymers: mechanism of action, factors of activity, and applications. *Appl. Microbiol. Biotechnol.* **2011**, 89 (3), 475–492.
- (63) Helander, I. M.; Mattila-Sandholm, T. Fluorometric assessment of Gram-negative bacterial permeabilization. *J. Appl. Microbiol.* **2000**, 88 (2), 213–219.
- (64) Chen, C. Z. S.; Cooper, S. L. Interactions between dendrimer biocides and bacterial membranes. *Biomaterials* **2002**, *23* (16), 3359–3368
- (65) Engler, A. C.; Wiradharma, N.; Ong, Z. Y.; Coady, D. J.; Hedrick, J. L.; Yang, Y. Y. Emerging trends in macromolecular antimicrobials to fight multi-drug-resistant infections. *Nano Today* **2012**, 7 (3), 201–222.
- (66) Opekarova, M.; Tanner, W. Specific lipid requirements of membrane proteins a putative bottleneck in heterologous expression. *Biochim. Biophys. Acta, Biomembr.* **2003**, *1610* (1), 11–22.
- (67) Epand, R. M.; Epand, R. F. Lipid domains in bacterial membranes and the action of antimicrobial agents. *Biochim. Biophys. Acta, Biomembr.* **2009**, *1788* (1), 289–294.
- (68) Goldfine, H. Bacterial-membranes and lipid packing theory. *J. Lipid Res.* **1984**, 25 (13), 1501–1507.
- (69) Yang, L. H.; Gordon, V. D.; Trinkle, D. R.; Schmidt, N. W.; Davis, M. A.; DeVries, C.; Som, A.; Cronan, J. E.; Tew, G. N.; Wong, G. C. L. Mechanism of a prototypical synthetic membrane-active antimicrobial: Efficient hole-punching via interaction with negative

- intrinsic curvature lipids. Proc. Natl. Acad. Sci. U. S. A. 2008, 105 (52), 20595–20600.
- (70) Som, A.; Yang, L.; Wong, G. C. L.; Tew, G. N. Divalent Metal Ion Triggered Activity of a Synthetic Antimicrobial in Cardiolipin Membranes. *J. Am. Chem. Soc.* **2009**, *131* (42), 15102–15103.
- (71) Wimley, W. C. Describing the mechanism of antimicrobial peptide action with the interfacial activity model. *ACS Chem. Biol.* **2010**, *5* (10), 905–917.
- (72) Liang, H. J.; Whited, G.; Nguyen, C.; Stucky, G. D. The directed cooperative assembly of proteorhodopsin into 2D and 3D polarized arrays. *Proc. Natl. Acad. Sci. U. S. A.* **2007**, *104* (20), 8212–8217.
- (73) Turner, D. C.; Gruner, S. M. X-Ray-Diffraction Reconstitution of the Inverted Hexagonal ( $H_{\rm II}$ ) Phase in Lipid Water-Systems. *Biochemistry* **1992**, *31* (5), 1340–1355.